RSC Advances

ROYAL SOCIETY OF CHEMISTRY

www.rsc.org/advances

Journal Name

COMMUNICATION

Photoelectrochemical deposited Sb_2Se_3 thin films: deposition mechanism and characterization†

Received 00th January 20xx,
Accepted 00th January 20xx

DOI: 10.1039/x0xx00000x

www.rsc.org/

Jia Yang,[a] Yanqing Lai,*[a] Yanyun Fan,[a] Yan Jiang,[a] Ding Tang,[a] Liangxing Jiang,[a] Fangyang Liu,*[a] Jie Lia[a]

Sb_2Se_3 thin films were photoelectrochemical deposited (PED) with compelling photoelectrochemical (PEC) performance. The main influence mechanism of illumination on Sb_2Se_3 deposition is that photoconductive effect accelerates the deposition rate and photogenerated electron (in conduction band of deposited Sb_2Se_3 thin film) promotes the electroreduction of SbO^+. Electrochemical impedance spectroscopy (EIS) and potentiostatic polarization show the evidence that illumination can promote the rate of cathodic reduction. Linear sweep photovoltammetry (LSPV) and X-ray Fluorescence spectrometer (XRF) indicate that illumination is facilitated to the reduction of SbO^+. PED process can improve the homogeneity and compactness of the films, facilitate the growth of stoichiometric Sb_2Se_3 and further enhance the photocurrent response of films, compared to conventional electrochemical deposition (CED) process.

Sb_2Se_3 is widely considered as a new non-toxic and earth-abundant light absorber with excellent light absorption coefficient (>10^5 cm^{-1} at short wavelength) and suitable band gap (approximately 1.1~1.3 eV)[1, 2]. It is benefit for low-cost and large-scale production of thin film solar cells. Additionally, sensitized cell[3, 4], solid-state cell[5] and photoelectrochemical cell[6] based on Sb_2Se_3 (or Sb_2S_3) thin films have been fabricated with good performance, which draws a worldwide attention on its photoresponse property.

Several methods have been employed to fabricate Sb_2Se_3 thin films, such as vacuum thermal evaporation[5], chemical bath deposition[7], successive ionic layer adsorption and reaction methods[8], spray pyrolysis[9], pulsed laser deposition[10] and electrochemical deposition[3, 11-13]. Among these methods, electrochemical deposition (or electrodeposition) is reported as a very simple[14] and versatile[3] process to semiconductor film fabrication for the sake of economic and convenient considerations. However, due to different deposition potentials for various ions, it is difficult to control composition[15] for compound semiconductor electrodeposition. Low conductive semiconductor grown on cathode also leads to some problems[16] such as low growth rate, increasing ohmic potential drop at electrode during deposition.

Photoelectrochemical deposition (PED) is developing as a general preparative strategy, opening up new avenues on the synthesis of compound semiconductors. Due to the photosensitivity of deposited semiconductor films[15, 17-20], illumination would make a great influence on the enhancement of deposition current and the inhibition of ohmic potential drop at electrode. Therefore PED process has attracted researchers' attention and has been explored by many groups[16, 19, 21-26]. We have also conducted an earlier research[16] that demonstrates the PED process benefits high quality and well performing $CuInSe_2$ semiconductor thin film fabrication. This paper is mainly focused on revealing the deposition mechanism and characterizing the affections of illumination on electrodeposited Sb_2Se_3 thin films.

According to the transmittance of electrolyte solution (ESI†, Fig. S1), light in the wavelength range of 900 ~ 2000 nm with a low transmittance value is absorpted by electrolyte solutions for calefaction (photothermal effect)[27], but light in the wavelength range of 300~900 nm with a very high transmittance value can be absorbed by as-deposited films for exciting electrons and holes[16, 19] (photoelectric effect). For xenon lamp spectra, light in the wavelength range of 300~900 nm covers almost total emitted light energy[28]. Consequently, the influence of illumination on electrochemical behavior is dominated by photoelectric effect rather than photothermal effect.

The potential-energy diagram drawn in Fig. 1 illustrates the photoelectric effects of the illumination on Sb_2Se_3 electrodeposition mechanisms. Relative position of the conduction and valence band edges in Sb_2Se_3 layer is adopted from literature[29]. The beginning reduction potential of H_2SeO_3 and SbO^+ are at about 0.05 V and -0.43 V, respectively and thereby the deposition of Sb is more difficult[14] than that of Se. Once Sb_2Se_3 is potentiostatic cathodic deposited (e. g. at -0.55 V) on the surface of cathode, the Fermi level

[a]School of Metallurgy and Environment, Central South University, Changsha 410083, China. E-mail: laiyanqingcsu@163.com(Yanqing Lai) E-mail: liufangyang@csu.edu.cn(Fangyang Liu); fax: +86 0731 88710171; Tel: +86 731 88830649.

† Electronic Supplementary Information (ESI) available: The transmittance of electrolytes, potentiostatic polarization curves for deposition process, SEM and visual photographs for deposited films. See DOI: 10.1039/x0xx00000x

of Sb_2Se_3 will move along the positive direction to a location equal to this cathodic potential. Thus a band alignment in deposited Sb_2Se_3 favors electrons flowing from conduction band to electrolyte, and holes injecting into valence band from electrolyte. The driving force for electroreduction of SbO^+ and H_2SeO_3 is given by the difference between the Fermi level of deposited Sb_2Se_3 and the relevant redox potential in electrolyte.

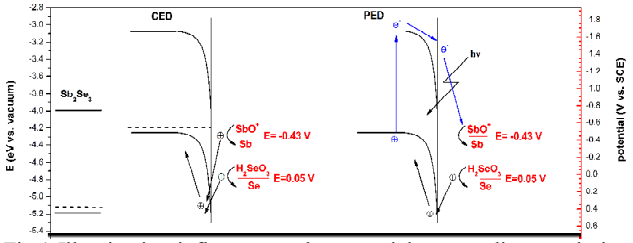

Fig.1 Illumination influence on the potential-energy diagram during Sb_2Se_3 electrodeposition.

In conventional electrochemical deposition (CED) process, majority carriers (holes) and very few minority carriers (electrons at conduction band) exist in p-type Sb_2Se_3, which means that only holes act as charge carriers and the electroreduction is inhibited by deposited Sb_2Se_3. The only reduction route is that positive charges inject into Sb_2Se_3 film from H_2SeO_3 and SbO^+. And the difference of energy level between the surface valance band and the redoxes is energy barrier for electroreduction of H_2SeO_3 and SbO^+. It is noteworthy that the reduction of SbO^+ is much more difficult than that of H_2SeO_3, because the SbO^+/Sb redox has higher energy barrier and lower driving force relative to the H_2SeO_3/Se redox.

In PED process, both the majority carriers (holes and photogenerated holes) and minority carriers (photogenerated electrons) act as charge carriers. And the photogenerated holes and photogenerated electrons will improve the conductivity[20] (photoconductive effect) of cathode and inhibit the actual potential drop (for potentiostatic electrodeposition) of film/electrolyte interface. Therefore, compared to CED process, the electroreduction of species in the electrolyte will be enhanced and the Sb_2Se_3 growth rate can be promoted accordingly. What is more, SbO^+ could receive photogenerated electrons from conduction band directly, driven by the bending band without any energy barrier, and be easily reduced to Sb. And the newly formed Sb may further react with electroreduced Se proceeded by Eq. (1) due to large Gibbs energy release (-135kJ/mol)[30], which further accelerates the deposition rate.

$$2Sb + 3Se = Sb_2Se_3 \quad (1)$$

Consequently, the potential-energy diagram may draw a conclusion that there are two affections of illumination on electrodeposition Sb_2Se_3: the first is accelerating the deposition rate; the second is promoting the electroreduction of SbO^+ by changing the electroreduction route.

To understand the underlying mechanism, Fig. 2 shows the Nyquist plots of CED process (a) and PED process (b) after different time of potentiostatic polarization (at -0.55 V). The main EIS difference between the CED process and PED process is that there exists an obviouse low-frequency Warburg diffusion resistance in the Nyquist plot of the latter. The difference of EIS indicates CED process is electroreduction control while PED process is electroreduction and diffusion simultaneously control[31-33]. Combined with smaller diameter of high-frequency semcirecle, these phenomena give a conclusion that electroreduction rate in PED process is faster than that in CED process. An equivalent circuit (Fig.2 (c)) is also designed to simulate the deposition[33] occurring at the cathode/electrolyte interface. R_{ct} is charge transfer resistance of cathode/electrolyte interface, C is the capacitance of the electrical double layer at the electrode, R_s is the ohmic resistance of electrolyte and W_s is Warburg diffusion resistance respectively.

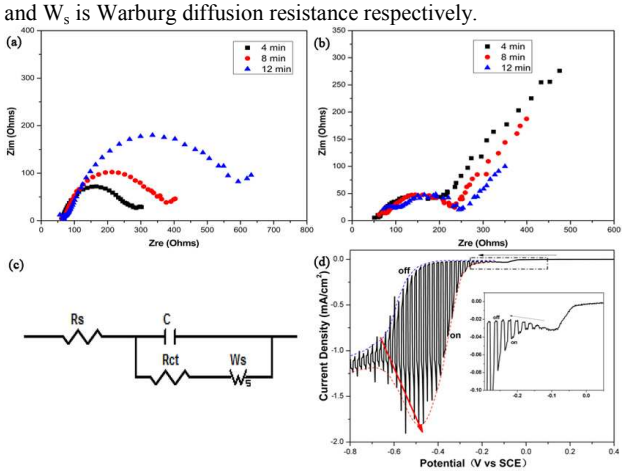

Fig 2. Nyquist plots of (a) CED process and (b) PED process after different time of potentiostatic polarization; (c) Equivalent circuit designed to simulate the deposition; (d) Linear sweep photovoltammogram on SnO_2 substrate under chopped illumination at scan rate of 2 mV/s (black solid line is measured value; blue/red dashed line is fitted value under dark/illumination respectively).

The values of R_{ct}, C, R_s and W_s for both of the systems are illustrated in Table 1.

Table 1 Parameters used for fitting the EIS data in Figure 2(a) and (b)

	CED			PED		
	4 min	8 min	12 min	4 min	8 min	12 min
R_{ct}	145.2	221.3	531.3	117.7	158.4	171.7
C	1.1E-04	1.0E-04	1.4E-04	7.4E-05	7.8E-05	6.6E-05
R_s	59.2	58.6	55.4	57.5	67.7	84.1
W_s	113.4	102.3	129.3	665.2	270.6	197.3

For CED process, with the increase of polarization time, the R_s and W_s of CED process remain relatively steady (below 60 Ω and about 110 Ω, respectively), which can be interpretated by the relatively steady electrolyte status. However, the diameters of capacitive semicircles obviously increase and R_{ct} increases accordingly (145.2 Ω for 4 min, 221.3 Ω for 8 min and 531.3 Ω for 12 min) due to the decrease in conductivity of the cathode (low electrical conductive Sb_2Se_3[34] covering, about $10^{-6} \sim 10^{-2}$ $\Omega^{-1}\cdot m^{-1}$).

For PED process, photogenerated carriers promote the cathodic reduction and further results in lower R_{ct}[32] (117.7 Ω for 4 min, 158.4 Ω for 8 min and 171.7 Ω for 12 min) than that for CED process. The C for PED (70 μF/cm^2) is lower than that for CED (100 μF/cm^2) probably due to the smoother surface (ESI†, Fig. S3) of PED thin film. However, with the increase of polarization time, the slightly increase of R_{ct} (from 117.7 Ω to 171.7 Ω) still relates to the

deposited film with low electrical conductivity (even under illumination), the R_s increases[35] (from 57.5 Ω to 84.1 Ω) can be attribute to ion consumption in electrolyte and the W_s decreases (from 665.2 Ω to 197.3 Ω) mainly results from the low concentration gradient.

Fig. 2 (d) shows the linear sweep photovoltammogram under chopped illumination from 0.40 V to -0.80 V (negative scanning) with an interval of 5 s. The curve displays an initial reduction peak at about -0.09 V which can be assigned to the four-electron predeposition of selenium[14, 24]. The reduction peak around -0.65 V (blue dash line, off) mainly corresponds to the reduction of SbO^+ and the subsequently formation of Sb_2Se_3[14, 24], which positively shifts to -0.48 V under illumination (red dash line, on). The 0.17 V positive shift of reductive peak indicates that the illumination facilitates the reduction of SbO^+ (also shown in Fig. 1). In addition, a higher current density is obtained, indicating that the reduction of SbO^+ and the accordingly formation of Sb_2Se_3 can be significantly promoted under illumination.

The largest photocurrent response is observed at potential between −0.45 V and −0.55 V, revealing that the significant influence of illumination on Sb_2Se_3 film deposition can be observed at this potential region. So Sb_2Se_3 was deposited at −0.45 V and −0.55 V for further research.

The composition analysis by XRF shows that Sb content is higher in PED Sb_2Se_3 films (41.09 at%, deposited at -0.45 V and 44.10 at%, deposited at -0.55 V) than that in CED Sb_2Se_3 films (4.87 at%, deposited at -0.45 V and 22.04 at%, deposited at -0.55 V). This finding furnishes additional evidence in support of the illumination promoting the electroreduction of SbO^+ with more negative reduction potential compared to H_2SeO_3. Moreover, films with near stoichiometry of Sb: Se=2: 3 can be easily obtained by PED process.

The enhanced deposition rate of Sb_2Se_3 can be also verified by the higher deposition current (ESI†, Fig. S2) and the thicker film obtained under illumination. The thicknesses of films are 0.05 μm/0.60 μm deposited at -0.45 V and 0.1 μm/0.70 μm deposited at -0.55 V for CED/PED, respectively. From the SEM micrographs (ESI†, showed in Fig. S3), it can be observed that PED Sb_2Se_3 films have more homogeneous and smooth morphology. According to the analysis of visual photographs (ESI†, showed in Fig. S3 insert), -0.55 V is benefical to film deposition. Because the films electrodeposited at -0.45 V are much more transparent than ones electrodeposited at -0.55 V.

Fig. 3 (a) shows the Raman spectroscopy of the Sb_2Se_3 films deposited by PED and CED at -0.55 V. The characteristic peaks coming from Sb_2Se_3 can be observed[36-41]: 83 cm^{-1}, 118 cm^{-1}, 189 cm^{-1}, 253 cm^{-1}, 372 cm^{-1} and 450 cm^{-1}. All peaks of PED film exhibit narrower peak width (more acute shape) and greater peak intensity than those of CED film, generally indicating the enhancement of crystallinity[41, 42]. The main peaks at about 189 cm^{-1} and 253 cm^{-1} correspond to the vibrations[36, 41] related to Sb bonds. Therefore, the obvious enhancement of main peak intensity should be related to the increase of Sb content (from 22.1 at% to 44.1 at%).

The XRD patterns of CED and PED Sb_2Se_3 thin films (on SnO_2/glass) after RTA (rapid thermal annealing treatment) are shown in Fig. 3(b). It can be seen that polycrystalline films of antimonselite phase[4] (Sb_2Se_3 (JCPDS No. 65-2433)) are achieved for both CED and PED thin films. The intensity of SnO_2 (JCPDS No. 77-0452) diffraction peaks for PED thin film is weaker than that for CED thin film, due to the difference thickness of two kinds of films. We can also notice that the Sb_2Se_3 diffraction intensity of PED thin film is stronger than that of CED thin film, indicating an improvement in crystalline quality by photoelectrochemical deposition. Similar phenomena have also been reported[43]. The improvement in crystalline quality can partly related to the difference of antimony content in these two kinds of films[44].

The absorption coefficient α and optical band gap (in insert, estimated from the interception of the linear fitting) of the CED and PED Sb_2Se_3 films are both shown in Fig. 3(c). Because the component of CED Sb_2Se_3 film deviates from stoichiometry, film shows a low absorption coefficient α (about 8×10^4 cm^{-1} in visible light) and narrow band gap value (0.93 eV). While PED Sb_2Se_3 film shows excellent optical property (absorption coefficient $\alpha \approx 1.4\times10^5$ cm^{-1} in visible light, band gap value =1.37 eV) close to the value of single crystal Sb_2Se_3[45, 46]. This excellent optical property can meet the need for the thin film solar cell materials[47].

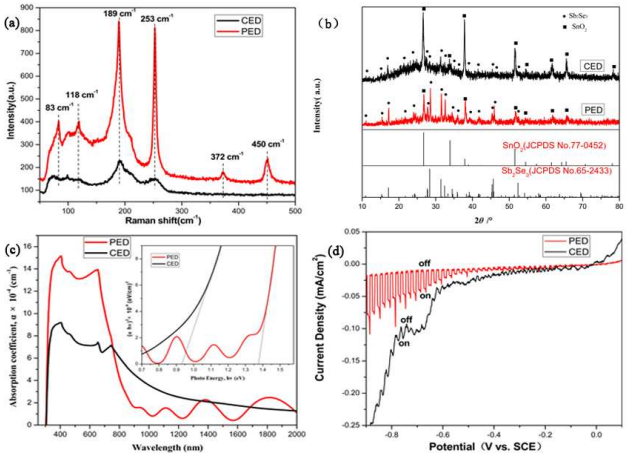

Fig.3 (a) Raman patterns of Sb_2Se_3 thin films prepared by PED and CED at -0.55 V; (b)X-ray diffraction patterns of CED and PED Sb_2Se_3 samples after RTA; (c) The optical characteristics of as-deposited Sb_2Se_3 films prepared by PED and CED. The inset shows the estimated optical band gap; (d) Photocurrent–potential response curve of the Sb_2Se_3 films prepared by PED (red line) and CED (black line) in 0.5M H_2SO_4.

The obviously difference on the PEC performance of PED and that of CED Sb_2Se_3 films is showed in Fig. 3 (d). Both the films are identified as p-type semiconductor due to the photocurrent densities increase with negative shift of the cathodic potential. At negative bias, the dark current (off) of PED film is lower than that of CED film, implying that PED film shows better rectification[48]. Since the rectification behaviour is considered to be limited by the deficiency, we may conclude that the deficiency (exposed substrate, impurities (undetected excess Se phase), crack or boundary between the granules) in PED film is much less than that in CED film. This conclusion is in accordance with the compact morphology and near stoichiometry for PED sample.

To confirm the conductivity of the deposited Sb_2Se_3 thin films again, photovoltage measurement[49, 50] was employed by determining the difference between the illuminated and dark voltages of the Sb_2Se_3 electrode with respect to the counter electrode. The p- and n-type silicon wafers were used for comparison and calibration of the

system. It is shown from Table 2 that a positive photovoltage demonstrates the p-type bulk conductivity of deposited Sb_2Se_3 thin films. In agreement with the difference of photocurrent, PED Sb_2Se_3 thin film has a higher photovoltage than that CED Sb_2Se_3 thin film has.

Based on the above analysis, PED and CED Sb_2Se_3 films are both identified as p-type semiconductor. Stronger and more sensitive photoresponse suggest PED Sb_2Se_3 film has better ability of photon-to-electron conversion.

Table 1 Photovoltage produced at the Sb_2Se_3 electrode/electrolyte junction during light illumination.

sample	measurement		analysis	
	V_{dark} / mV	V_{light} / mV	V_{photo} / mV	conductivity
p-Si	-615	-573	42	p-type
n-Si	-330	-507	-177	n-type
PED	-352	-265	87	p-type
CED	-371	-359	12	p-type

Conclusions

This work demonstrates the beneficial affections of illumination on Sb_2Se_3 electrodeposition. The influence mechanism has been illustrated by schematic diagram and been borne out by many experiments: the electroreduction of SbO^+ with more negative reduction potential is promoted and the deposition rate of Sb_2Se_3 gets further increased. Moreover, PED improves content of antimony, homogeneity, compactness in morphology and Sb_2Se_3 crystallinity. As a result, Sb_2Se_3 films with excellent optical property and ability of photon-to-electron conversion can be obtained by PED. Accordingly, PED is indeed a very competitive strategy and PED Sb_2Se_3 film should be more suitable for high efficiency solar cells application.

Experimental Section

Deposition and analysis

Electrochemical experiments were carried out in a stagnant three-electrode Pyrex electrolytic cell configuration at 25□ with a SnO_2-coated glass substrate (SnO_2/glass, 20 Ω/sq) as working electrode, a Pt gauze as counter electrode, and a saturated calomel electrode (SCE) as reference electrode. All potentials were reported with respect to this reference electrode. The SnO_2/glass substrates were ultrasonically cleaned in acetone, ammonia and alcohol, then rinsed with deionized water (18.2 $M\Omega \cdot cm^{-1}$), and subsequently dried in nitrogen flow. Linear sweep photovoltammetry (LSPV), PED and CED were performed by Princeton Applied Research PARSTAT 4000 Potentiostat, and the electrochemical impedance spectroscopy (EIS) were performed using a Princeton Applied Research PARSTAT 4000 EIS analyzer. The electrolyte solution containing 5.5 mM $K(SbO)C_4H_4O_6 \cdot 0.5H_2O$ (antimony potassium tartrate), 4.5 mM H_2SeO_3, and 100 mM NH_4Cl was used for LSPV, PED, CED and EIS. The pH of the electrolyte solution was adjusted to 2.3 using concentrated hydrochloric acid. The linear sweep photovoltammogram was measured at a scan rate of 2 mV/s under chopped illumination. Sb_2Se_3 films were prepared by PED and CED and all the films were deposited for 30 mins potentiostatically. EIS measurement was carried out under the amplitude of 10 mV at -0.55 V with a frequency range of 100 kHz ~ 0.1 Hz. When it was necessary, A Newport 300 W xenon lamp was used as the light source with the light intensity kept at 100 mW/cm^2.

Characterizations

Chemical composition, morphology and phase of the film were characterized by energy dispersive X-ray Fluorescence spectrometer (XRF, Shimadzu, LAB CENTER XRF-1800, operated at 40 kV, 95 mA), environmental scanning electron microscopy (ESEM, FEI Quanta-200, at a 20-keV accelerating voltage) and Raman spectrometer (Jobin-Yvon LabRAM HR-800, Horiba), respectively. Thickness of the film was measured using a Veeco Dektak 150 surface profiler. The crystalline properties of the prepared films after RTA (rapid thermal annealing treatment in the flowing Ar atmosphere (20.00 sccm) at 300□ for 3 min) were characterized by an X-ray diffractometer (XRD, Rigaku3014). Optical property of the films and electrolytes were measured by UV-VIS-NIR spectrophotometer (UV-VIS-NIR, Varian Cary-5000) in a wavelength range of 300 nm~2000 nm at room temperature.

Photoelectrochemical (PEC) property was performed in three-electrode configuration containing 0.5 M H_2SO_4 solution (also at a scan rate of 2 mV/s, under chopped illumination) for the ability of photon-to-electron conversion by Princeton Applied Research PARSTAT 4000 Potentiostat. The three-electrode configuration consisted of a Sb_2Se_3 deposited on SnO_2/glass, a Pt gauze and a saturated calomel electrode (SCE), acting as working electrode, counter electrode and reference electrode, respectively. Photovoltage measurement was performed in the two-electrode configuration only consisted of working electrode (a Sb_2Se_3 deposited on SnO_2/glass) and counter electrode (a Pt gauze).

Acknowledgements

This work was supported by The National Natural Science Foundation of China (Grant No. 51222403 and 51272292) and Hunan Provincial Natural Science Foundation of China (13JJ1003).

Notes and references

1. M. R. Filip, C. E. Patrick and F. Giustino, *Phy. Rev. B*, 2013, **87**, 205125.
2. C. E. Patrick and F. Giustino, *Adv. Funct. Mater.*, 2011, **21**, 4663-4667.
3. T. T. Ngo, S. Chavhan, I. Kosta, O. Miguel, H.-J. Grande and R. Tena-Zaera, *ACS Appl. Mater. Inter.*, 2014, **6**, 2836-2841.
4. S. H. Im, C.-S. Lim, J. A. Chang, Y. H. Lee, N. Maiti, H.-J. Kim, M. K. Nazeeruddin, M. Grätzel and S. I. Seok, *Nano Lett.*, 2011, **11**, 4789-4793.
5. Y. Zhou, L. Wang, S. Chen, S. Qin, X. Liu, J. Chen, D.-J. Xue, M. Luo, Y. Cao, Y. Cheng, E. H. Sargent and J. Tang, *Nature Photon.*, 2015, **9**, 409-415.
6. B. R. Sankapal and C. D. Lokhande, *Sol. Energy Mater. Sol. Cells*, 2001, **69**, 43-52.
7. Y. Rodríguez-Lazcano, Y. Peña, M. T. S. Nair and P. K. Nair, *Thin Solid Films*, 2005, **493**, 77-82.

8. C. D. Lokhande, B. R. Sankapal, S. D. Sartale, H. M. Pathan, M. Giersig, and V. Ganesan, *Appl. Surf. Sci.*, 2001, **182**, 413-417.
9. K. Y. Rajpure and C. H. Bhosale, *Phys. Chem. Minerals*, 2000, **62**, 169-174.
10. M.-Z. Xue and Z.-W. Fu, *J. Alloys Compd.*, 2008, **458**, 351-356.
11. A. M. Fernandez and M. G. Merino, *Thin Solid Films*, 2000, **366**, 202-206.
12. A. P. Torane and C. H. Bhosale, *J. Phys. Chem. Solids*, 2002, **63**, 1849-1855.
13. A. P. Torane, K. Y. Rajpure and C. H. Bhosale, *mater. chem. phys.*, 1999, **61**, 219-222.
14. Y. Lai, C. Han, X. Lv, J. Yang, F. Liu, J. Li and Y. Liu, *J. Electroanalytical Chem.*, 2012, **671**, 73-79.
15. C.-H. Wang, K.-W. Cheng and C.-J. Tseng, *Sol. Energy Mater. Sol. Cells*, 2011, **95**, 453-461.
16. J. Yang, F. Liu, Y. Lai, J. Li and Y. Liu, *Electrochem. Solid-State Lett.*, 2012, **15**, D19.
17. R. N. Bhattacharya, W. Batchelor, K. Ramanathan, M. A. Contreras and T. Moriarty, *Sol. Energy Mater. Sol. Cells*, 2000, **63**, 367-374.
18. M. Izaki, T. Shinagawa, K.-T. Mizuno, Y. Ida, M. Inaba and A. Tasaka, *J. Phys. D: Appl. Phys.*, 2007, **40**, 3326-3329.
19. K. Murase, M. Matsui, M. Miyake, T. Hirato and Y. Awakura, *J. Electrochem. Soc.*, 2003, **150**, C44.
20. H. L. Porter, A. L. Cai, J. F. Muth and J. Narayan, *Appl. Phys. Lett.*, 2005, **86**, 211918.
21. M. B. Dergacheva, K. A. Urazov and K. A. Leont'eva, *Russ. J. Appl. Chem.*, 2014, **87**, 724-729.
22. K. Kamada, K. Higashikawa, M. Inada, N. Enomoto and J. Hojo, *J. Phys. Chem. C*, 2007, **111**, 14508-14513.
23. A. Lahiri, S. Zein El Abedin and F. Endres, *J. Phys. Chem. C*, 2012, **116**, 17739-17745.
24. Y. Matsumoto, M. Noguchi and T. Matsunaga, *J. Phys. Chem. B*, 1999, **103**, 7190-7194.
25. S. Somasundaram, C. R. Chenthamarakshan, N. R. d. Tacconi, Y. Ming and K. Rajeshwar, *Chem. Mater.*, 2004, **16**, 3846-3852.
26. M. Takahashi, M. Todorobaru, K. Wakita and K. Uosaki, *Appl. Phys. Lett.*, 2002, **80**, 2117.
27. N. A. Marley, J. S. Gaffney and M. M. Cunningham, *Environ. Sci. Technol.*, 1993, **27**, 2864-2869.
28. https://en.wikipedia.org/wiki/Xenon_arc_lamp).
29. X. Liu, J. Chen, M. Luo, M. Leng, Z. Xia, Y. Zhou, S. Qin, D.-J. Xue, L. Lv, H. Huang, D. Niu and J. Tang, *ACS Appl. Mater. Interfaces*, 2014, **6**, 10687-10695.
30. G. Ghosh, *J. phase equilib.*, 1993, **14**, 753-763.
31. F.-H. Li, W. Wang, J.-P. Gao and S.-Y. Wang, *J. Electrochem. Soc.*, 2009, **156**, D84.
32. I. Danaee, *J. Electroanalytical Chem.*, 2011, **662**, 415-420.
33. M. A. Pasquale, L. M. Gassa and A. J. Arvia, *Electrochim. Acta*, 2008, **53**, 5891-5904.
34. D. Choi, Y. Jang, J. Lee, G. H. Jeong, D. Whang, S. W. Hwang, K.-S. Cho and S.-W. Kim, *Sci. Rep.*, 2014, **4**, 6714.
35. J. Bobacka, A. Lewenstam and A. Ivaska, *J. Electroanalytical Chem.*, 2000, **489**, 17-27.
36. Z. G. Ivanova, E. Cernoskova, V. S. Vassilev and S. V. Boycheva, *Mater. Lett.*, 2003, **57**, 1025– 1028.
37. J. Lu, Q. Han, X. Yang, L. Lu and X. Wang, *Mater. Lett.*, 2008, **62**, 2415-2418.
38. X. Ma, Z. Zhang, X. Wang, S. Wang, F. Xu and Y. Qian, *J. Cryst. Growth*, 2004, **263**, 491-497.
39. J. Wang, Z. Deng and Y. Li, *Mater. Res. Bull.*, 2002, **37**, 495-502.
40. T. Zhai, M. Ye, L. Li, X. Fang, M. Liao, Y. Li, Y. Koide, Y. Bando and D. Golberg, *Adv. Mater.*, 2010, **22**, 4530-4533.
41. Y. Zhang, G. Li, B. Zhang and L. Zhang, *Mater. Lett.*, 2004, **58**, 2279-2282.
42. O. Ramdani, J. F. Guillemoles, D. Lincot, P. P. Grand, E. Chassaing, O. Kerrec and E. Rzepka, *Thin Solid Films*, 2007, **515**, 5909-5912.
43. Y.-H. Su, T.-W. Chang, W.-H. Lee and B.-H. Tseng, *Thin Solid Films*, 2013, **535**, 343-347.
44. D. Tang, J. Yang, F. Liu, Y. Lai, J. Li and Y. Liu, *Electrochim. Acta*, 2012, **76**, 480-486.
45. F. Kosek, J. Tulka and Š. L, *Czech. J. Phys. B*, 1978, **28**, 325-330.
46. M. Leng, M. Luo, C. Chen, S. Qin, J. Chen, J. Zhong and J. Tang, *Appl. Phys. Lett.*, 2014, **105**, 083905.
47. A. Goetzberger, C. Hebling and H. W. Schock, *Materials Science and Engineering: R: Reports*, 2003, **40**, 1-46.
48. H. Ye, H. S. Park and V. A. Akhavan, *J. Phys. Chem. C*, 2010, **115**, 234-240.
49. I. M. Dharmadasaz, N. B. Chaure, G. J. Tolan and A. P. Samantilleke, *J. Electrochem. Soc.*, 2007, **154**, H466-H471.
50. T. Delsol, A. P. Samantilleke, N. B. Chaure, P. H. Gardiner, M. Simmonds and I. M. Dharmadasa, *Sol. Energy Mater. Sol. Cells*, 2004, **82**, 587-599.

Photoelectrochemical deposited Sb_2Se_3 thin films present interesting properties and performance with accelerated deposition rate and changed electroreduction route of SbO^+, suggesting that this deposition technology should result in the settlement of the dilemma of compound semiconductor electrodeposition.